PCCP

PAPER

View Article Online
View Journal | View Issue

Cite this: *Phys. Chem. Chem. Phys.*, 2022, **24**, 18888

Electrochemical impedance and X-ray absorption spectroscopy analyses of degradation in dye-sensitized solar cells containing cobalt tris(bipyridine) redox shuttles†

Jiajia Gao,[a] Aleksandar Tot,[a] Haining Tian,[b] James M. Gardner,[a] Dibya Phuyal[c] and Lars Kloo *[a]

Electrochemical impedance spectroscopy (EIS) is a commonly used steady-state technique to examine the internal resistance of electron-transfer processes in solar cell devices, and the results are directly related to the photovoltaic performance. In this study, EIS was performed to study the effects of accelerated ageing, aiming for insights into the degradation mechanisms of dye-sensitized solar cells (DSSCs) containing cobalt tris(bipyridine) complexes as redox mediators. Control experiments based on aged electrolytes differing in concentrations of the redox couple components and cation co-additives were conducted to reveal the correlation of the cell degradation with external and internal properties. The failure modes of the cells emerged as changes in the kinetics of charge- and ion-transfer processes. An insufficient concentration of the redox complexes, in particular Co(III), was found to be the main reason for the inferior performance after ageing. The related characterization of electrolytes aged outside the solar cell devices confirms the loss of active Co(III) complexes in the device electrolytes. A new EIS feature at low frequencies emerged during ageing and was analysed. The new EIS feature demonstrates the presence of an unexpected rate-limiting, charge-transfer process in aged devices, which can be attributed to the TiO_2/electrolyte interface. High-resolution fluorescence detected X-ray absorption spectroscopy (HERFD-XAS) was performed to identify the reduction of a part of Co(III) to Co(II) after ageing, by investigating the Co K absorption edge. The HERFD-XAS data suggested a partial reduction of Co(III) to Co(II), accompanied by a difference in symmetry of the reduced species.

Received 20th May 2022,
Accepted 18th July 2022

DOI: 10.1039/d2cp02283d

rsc.li/pccp

Introduction

In the area of photovoltaic (PV) technology development, the photon-to-current conversion efficiency of dye-sensitized solar cells (DSSCs) appears to have reached a plateau.[1] Currently, with the sudden emergence of other PV technologies, such as perovskite-type solar cells, DSSCs are faced with the threat of being phased out of competition. In order to overcome this situation, there are two ways to go: (1) improving the photovoltaic performance by broadening the spectral absorption of a sensitizer for high photocurrent and decreasing the electron–hole recombination loss for high photovoltage and (2) improving the long-term durability, which is the most demanding challenge also for other, new PV cell technologies before commercial applications can be considered realistic. For studies on the chemical stability, liquid DSSCs still represent a good model due to their well-studied mechanism of function and easily controlled constitution.

The function of a PV cell can be characterized by the photovoltaic performance and internal resistance, which are known as the combined results of kinetics and resistances of various rate-limiting, charge-transfer (CT) and mass transport processes in the cell. Therefore, changes in these processes must be taken into account in order to gain insights into the functional degradation of the solar cell. Correspondingly, the carriers of the charges, that is, the functional materials comprising the devices, must have undergone certain physical or chemical changes under the accelerated ageing conditions.[2–4] In order to visualize the nature of these changes, accurate

[a] *Division of Applied Physical Chemistry, Department of Chemistry, KTH Royal Institute of Technology, SE-100 44, Stockholm, Sweden. E-mail: Lakloo@kth.se*
[b] *Department of Chemistry, Ångström Laboratory, Uppsala University, Box 523, SE-75120, Uppsala, Sweden*
[c] *Department of Materials and Nanophysics, KTH Royal Institute of Technology, SE-100 44, Stockholm, Sweden*

† Electronic supplementary information (ESI) available: The experimental details, additional figures and tables including solar cell performance variations, transient absorption kinetic traces and fitting parameters, Tool-box, UV-vis and PIA spectroscopy results. See DOI: https://doi.org/10.1039/d2cp02283d

in situ or *ex situ* analytical methods and techniques are required but may still be insufficient to obtain full insights at a molecular level. Our previous work has revealed that the open-circuit voltage for DSSCs mediated by cobalt tris(bipyridine) complexes shows a steady decline during the ageing test. And it has been correlated with the lifetime attenuation of the electrons in TiO_2 due to the recombination of the electrolyte acceptors, and, in particular, the commonly used lithium ion additives accelerate the degradation, probably through promoting the light-induced consumption of dyes at the TiO_2 surface.[5] Ion diffusion in the electrolyte has also been claimed critical for the performance of liquid-type DSSCs. The stability studies of the traditional iodide/triiodide-based DSSCs have attributed the performance failure to the retarded diffusion as a result of the depletion of triiodide induced by UV light and/or thermal stress.[6,7] The concentration loss of the redox mediators resulting in an increase in the diffusion resistance limiting the DSSC performance was also argued to dominate in the stability studies of $Co(bpy)_3^{2+/3+}$-based DSSCs.[8]

Electrochemical impedance spectroscopy (EIS) is a powerful tool for mapping central physicochemical processes in a multi-interface electrochemical system. However, the correct modelling of the processes based on equivalent-circuit elements is required for an understanding of the recorded impedance signals. Based on the well-studied operation mechanism of liquid-type DSSCs, a general equivalent-circuit model (general transmission lines) consisting of a distribution of resistor–capacitor (RC) elements has been constructed and widely applied to analyze the EIS data.[9,10] This general model can be simplified by single RC elements in particular cases with an isotropic electrical response in the active layer and Ohmic contacts.[11] The charge transfer at the cathode is much faster than the electron recombination at the anode, and the impedance can be thus modelled as two RC elements in series for the two sequential relaxation processes. The typical simplified model for liquid-type DSSCs is shown as Model 1 in Scheme 1. This model consists of a series of resistances (R_s) accounting for contacting resistances, a charge-transfer (CT) resistance (R_{ct}) and a double-layer capacitance (C_{ce}) accounting for the high-frequency CT process at the electrolyte/counter electrode interface, the recombination resistance (R_{rec}) and chemical capacitance (C_μ) accounting for the intermediate-frequency electron recombination at the TiO_2/electrolyte interface and finally the Warburg impedance (WS) used to describe electrolyte diffusion at low frequencies. These circuit elements model a typical EIS feature for liquid-type DSSCs and manifest itself as three distorted semicircles in the Nyquist plot or alternatively as three peaks/plateaus in the Bode plot. In addition, the characteristic time constant of the CT processes can be extracted by using the relationship $t = RC$.[12]

In this work, we have employed EIS as the main tool to analyze the changes in aged cobalt-based DSSCs in an extended time scale. By controlling the external ageing conditions and internal electrolyte formulation, insights into the failure modes of this type of DSSCs and the ultimate causes are implicated. Interestingly, we note that when the ageing tests are prolonged, *e.g.* to several hundred hours, a new EIS feature appears at low frequencies. In order to model this feature, two new circuit elements denoted as R_{new} and C_{new} were added in series to the elements in Model 1, shown in Scheme 1 as model 2. Regarding the origin of this EIS signal, the present work reveals that it can be attributed to the aged electrolyte and processes at the electrolyte TiO_2 interface. X-ray absorption investigations have subsequently been used to identify the changes in Co-ion speciation associated with the observed degradation effects.

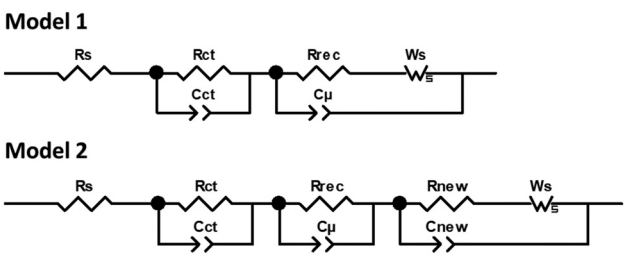

Scheme 1 The simplified equivalent-circuit models for liquid DSSCs: the commonly used model (model 1), and the model used for aged DSSCs in this work (model 2).

Experimental section

Materials

All chemicals were purchased from Sigma Aldrich unless otherwise noted: Fluorine-doped tin oxide (FTO; Pilkington, TEC 15 Ω cm^{-2} and TEC 7 Ω cm^{-2}), TiO_2 pastes (Dyesol Ltd, DSL 18NR-T and WER2-O), Surlyn frame (Solaronix), acetonitrile (Aldrich, 99.8%), 4-*tert*-butylpyridine (TBP; Aldrich, 96%), lithium perchlorate ($LiClO_4$; Aldrich, 99.99%), 1-ethyl-3-methylimidazolium tetracyanoborate (EIMTCB; Merck), potassium tetracyanoborate ($KB(CN)_4$; SelectLab, 97%), 1-butyl-3-methylimidazolium chloride (BIMCl; Aldrich, ≥98.0%), n-tetraethylammonium iodide (TEAI; Aldrich, 98%), n-tetrabutylammonium bromide (TBABr; Aldrich, ≥99.0%). The dye (D35) and the tetracyanoborate or hexafluorophosphate salts of tris(2, 2′-bipyridine-2N, N′) cobalt(II/III) were all obtained commercially. All chemicals were of reagent grade and used without further purification. The following chemicals were prepared according to relevant literature procedures:[13,14] 1-butyl-3-methylimidazolium tetracyanoborate (BIMTCB), *n*-tetraethylammonium tetracyanoborate (TEATCB), and *n*-tetrabutylammonium tetracyanoborate (TBATCB).

Solar cell fabrication and characterization

The details of solar cell fabrication have been reported previously.[15] A transparent TiO_2 layer (diluted paste: a mixture of 60 wt % TiO_2 paste (DSL 18NR-T) with 36 wt % terpineol and 4 wt % ethyl cellulose; area: 0.5 × 0.5 cm^2, thickness: 5 μm) and a scattering layer (WER2-O, 3 μm) were in succession screen-printed on a FTO substrate (Pilkington, TEC 15 Ω cm^{-2}) with a TiO_2 blocking layer pre-deposited by a simple hydrothermal method. The working electrodes were sintered under an ambient atmosphere (up to 325 °C for 25 min, thermostatic for 30 min, up to 500 °C for 25 min, thermostatic for 30 min and

natural cooling), and post-treated with an aqueous TiCl4 solution. All DSSCs fabricated and investigated in this work were sensitized by the classic dye D35; the structure is shown in Scheme S1 (ESI†). The working electrodes were dipped in a 0.25 mM D35/ethanol dye bath in the dark overnight to generate a dye-sensitizing layer. The platinized counter electrode was prepared by drop-casting 20 μl of 4.8 mM H_2PtCl_6 isopropanol solution on a pre-drilled and cleaned FTO (Pilkington, TEC 7 Ω cm^{-2}) glass substrate and then sintered in air at 400 °C for 30 min. The DSSCs were fabricated by assembling the sensitized TiO_2 electrodes with the Pt counter electrodes into a sandwich-type cell using a 25 μm thick hot-melt Surlyn frame (inner area: 0.6 × 0.6 cm^2) as the sealant, introducing the electrolyte through pre-drilled holes at an atmospheric pressure, and sealing using a 50 μm thermoplastic sheet and a glass coverslip. A metal contact was soldered on the edge of the FTO film to increase the conductivity. The electrolytes used consisted of $Co(bpy)_3^{2+/3+}$ and cation co-additives at different concentrations, as detailed below, and 0.2 M TBP in an acetonitrile solvent.

The current density–voltage (*J–V*) characteristics were measured using a light-shading metal mask (0.7 × 0.7 cm^2) on the top of the cell under standard irradiation (AM 1.5, 100 mW cm^{-2}) supplied using a Newport solar simulator (model 91160-1000). The *J–V* characteristics were investigated using a computerized Keithley 2400 source meter calibrated using a certified reference solar cell (Fraunhofer ISE). The stability tests were performed in a sample compartment under continuous irradiation (~100 mW cm^{-2}; ATLAS Suntest XLS) and a stable temperature at around 60 °C under open-circuit conditions and using a 390 nm UV cut-off filter. The characterization of the cells during ageing tests was performed using an ageing instrument at selected time intervals. The photovoltaic characteristics of the cells were measured by averaging the output from at least three devices for each electrolyte. UV-vis absorption spectra were recorded using a Cary 300 spectrophotometer in a quartz sample cell (0.5 cm path length). Differential pulse voltammetry (DPV) and cyclic voltammetry (CV) measurements were conducted using an Autolab potentiostat using a glassy carbon disk as the working electrode, a platinum wire as the counter electrode and $Ag/AgNO_3$ as the reference electrode. 0.1M $[Bu_4N]PF_6$ was added as a conductive medium. Electrochemical impedance spectroscopy (EIS) was performed using an Autolab PGstat12 potentiostat with an impedance module. EIS measurements were conducted in the dark at a bias voltage (−0.9 V) for all investigated systems to exclude the effects of the electron concentration in TiO_2 on the interfacial charge-transfer kinetics. The frequency was swept from 10^5 Hz to 0.1 Hz using a 20 mV AC amplitude. Resistances and capacitances were analysed using the software Z-View with fitting errors less than 10%.

High-resolution fluorescence detected X-ray absorption spectroscopy (HERFD-XAS) investigations at the Co K-edge were performed at the CLÆSS beamline[16] of the ALBA Synchrotron (Barcelona, Spain) using a Si (111) double-crystal monochromator. The spectra were recorded by monitoring the K_α (≈ 6930 eV) emission line and scanning the incident energy across the Co K absorption edge. The K_α fluorescence energy was selected using a Si (333) dynamical bent diced analyzer crystal and an energy dispersive one-dimensional (1D) detector in the Rowland circle geometry (Rowland radius = 1 m). The overall energy resolution was determined to be 0.8 eV from the full width at half-maximum (FWHM) of the quasi-elastic peak collected from the Kapton tape. The incident energy scale was calibrated and offset using a Co-metal foil.

As a reference Co(II/III) samples for the HERFD-XAS experiments, the solid CoO and $LiCoO_2$ were used. Solutions for the HEFRD-XAS experiments were as follows: (1) the high-spin Co(II) reference consisted of 0.1M $Co(bpy)_3(PF_6)_2$ in acetonitrile; (2) the low-spin Co(II) reference consisted of 0.1M $K_4[Co(CN)_6]$ in acetonitrile; (3) the Co(III) fresh sample consisted of 0.1M $Co(bpy)_3(PF_6)_3$ and 0.15M TBP in acetonitrile, and (4) the aged sample of Co(III) consisted of 0.1M $Co(bpy)_3(PF_6)_3$ and 0.15M TBP in acetonitrile after 1000 hours of illumination.

Results and discussion

Effects of cobalt redox concentrations

The loss of redox mediators under ageing conditions has been recognized for DSSC systems including iodide/triiodide-based and cobalt tris(bipyridine) complex based ones.[6–8] Therefore, we first investigated the effects of the concentration of $Co(bpy)_3^{2+/3+}$ initially added to the electrolyte on the device long-term performance. Table 1 lists the electrolytes investigated differing in the concentration of $Co(bpy)_3^{2+/3+}$ together with the initial device performance (Fig. S1, ESI†). Based on the commonly used composition (Co(II)/Co(III), 0.22 M/0.05 M), increasing the amount of either Co(II) or Co(III) leads to a slight decrease in the short-circuit current density (J_{sc}), while increasing the ratio of Co(III) in the total concentration of the cobalt salts leads to a better fill factor (FF). By comparing the 1000 h device performance of the investigated electrolytes (Fig. S2, ESI†), the conversion efficiency (η) shows a faster decline with a lower portion of Co(III) in the initial electrolyte. The correlation of η stability with the redox couple concentration ratio corresponds to those of J_{sc} and FF. EIS of the devices were recorded during the ageing test (Fig. S3 and S4, ESI†) and analyzed in

Table 1 The complex concentrations, concentration ratios and total concentration of $Co(bpy)_3^{2+/3+}$ in the electrolytes (A1–A4), and the corresponding photovoltaic performance of newly fabricated D35-sensitized solar cells

Electrolyte[a]	A1	A2	A3	A4
$[Co^{II}]$, $[Co^{III}]$/M	0.22, 0.05	0.30, 0.05	0.40, 0.05	0.30, 0.15
$[Co^{II}]/[Co^{III}]$	4.4 : 1	6 : 1	8 : 1	2 : 1
$[Co^{II/III}]_{total}$/M	0.27	0.35	0.45	0.45
J_{sc}/mA cm^{-2}	11.9 ± 0.2	11.6 ± 0.1	11.6 ± 0.1	11.4 ± 0.1
V_{oc}/V	0.89 ± 0.01	0.89 ± 0.00	0.89 ± 0.00	0.89 ± 0.01
FF	0.63 ± 0.01	0.62 ± 0.01	0.58 ± 0.00	0.65 ± 0.01
η/%	6.54 ± 0.27	6.37 ± 0.17	5.93 ± 0.10	6.54 ± 0.14

[a] All in acetonitrile solvent, and with the same co-additives: 0.1 M $LiClO_4$ and 0.2 M TBP.

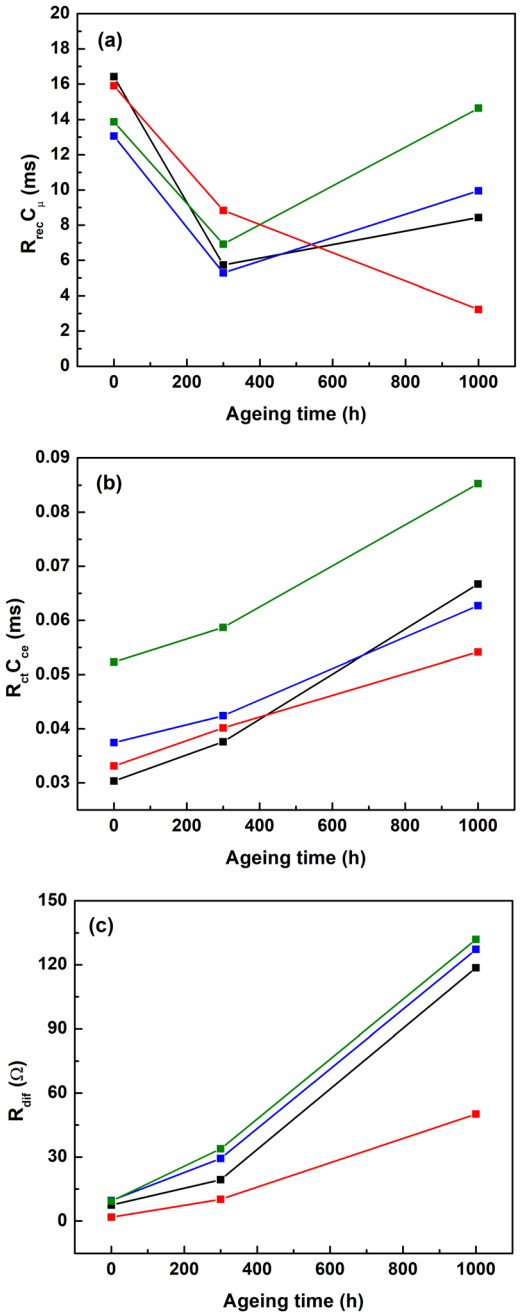

Fig. 1 The evolution of (a) $R_{rec}C_{\mu}$, (b) $R_{ct}C_{ce}$ and (c) R_{dif} with ageing times for DSSCs containing electrolytes differing in concentrations of $Co(bpy)_3^{2+/3+}$: A1, black; A2, blue; A3, green and A4, red. The data were extracted from the EIS results.

parallel. The changes in the kinetics of the crucial charge/ion-transfer processes for DSSCs were derived from the EIS data, as shown in Fig. 1 and Fig. S5 (ESI†). The electron lifetime (τ) in TiO_2 can be obtained by $\tau = R_{rec}C_{\mu}$ assuming a first-order, irreversible recombination process.[17,18] A general decrease in τ for all investigated electrolytes (Fig. 1a) accounts for the continuous degradation of the open-circuit voltage (V_{oc}), which has also been concluded in our previous work.[5] Particularly for DSSCs containing higher concentrations of Co(III), a better stability in J_{sc} and FF can be attributed to the slower increase in both the electrolyte diffusion resistance (R_{dif}) and the time constant of CT at the counter electrode/electrolyte interface ($R_{ct}C_{ce}$), see Fig. 1b and c. The diffusion of Co(III) dominates the effects of solute diffusion in the electrolyte as a whole due to its low and limiting concentration (lower than that of Co(II), and considering that Co(II) and Co(III) complexes display very similar diffusion coefficients).[15] Therefore, R_{dif} relies strongly on the concentration of Co(III) since the diffusion coefficient (D) of Co(III) negligibly changes during ageing.[19] It is also noted that R_{rec} and τ, which are also related to the concentration of Co(III) representing the recombination acceptors in the electrolyte, rebound in the later phase of the ageing test for cells containing lower concentration ratios of Co(III). Correspondingly, as shown by the Bode plots in Fig. S4 (ESI†), the characteristic response peak for the electron recombination process in the intermediate frequency region shifts and eventually overlaps with the low-frequency peak attributed to the electrolyte diffusion. Combining these facts to the observed correlation of FF with the concentration ratio of Co(III), we can deduce that the performance degradation of the cobalt-based DSSCs, which is particularly more dramatic for the electrolytes initially containing lower ratios of Co(III), is a result of the loss of redox-active Co(III) complexes during ageing. It has been confirmed by the gradual attenuation of 1H-NMR spectroscopy and electrochemical signals of Co(III) with the ageing time, see Figs. S6–S8 (ESI†).

New EIS feature

Based on the optimized electrolyte composition ((Co(II)/Co(III), 0.3 M/0.15 M) for the sake of the best device stability, a characteristic EIS peak emerges unexpectedly with prolonging the ageing test (>200–300 h) in Bode phase-angle plots (Fig. 2a). The new feature, which is located between the two originating from the TiO_2/electrolyte interfacial recombination (10–100 Hz) and ion-diffusion (<1 Hz) processes, can be regarded as the 4th peak/semicircle with respect to the typical EIS feature for new liquid-type DSSCs that normally include three phase peaks/semicircles. Notably, this new feature is more pronounced when the device aged under light irradiation (Fig. 2a and Fig. S9, ESI†). Besides the external ageing conditions, we also investigated the related effects of the internal composition of the electrolyte differing in the cation co-additives, since the addition of cation co-additives alters the properties of both the electrode surface and the electrolyte, and necessarily affects the related charge/ion-transfer kinetics. Herein, besides the commonly used lithium-ion co-additives ($LiClO_4$ in this work), other alternatives comprising different organic cations with a much lower charge-to-size ratio, such as ammonium cations (TEA^+ and TBA^+) and imidazolium cations (EIm^+ and BIm^+) were employed and compared to the electrolyte free of cation co-additives (A-free). The effects of the concentration of the cation co-additives were investigated as well based on the EIm^+-containing system. The initial photovoltaic performance of the corresponding devices is listed in Table S1 (ESI†). In Fig. S10 (ESI†), the new EIS feature was

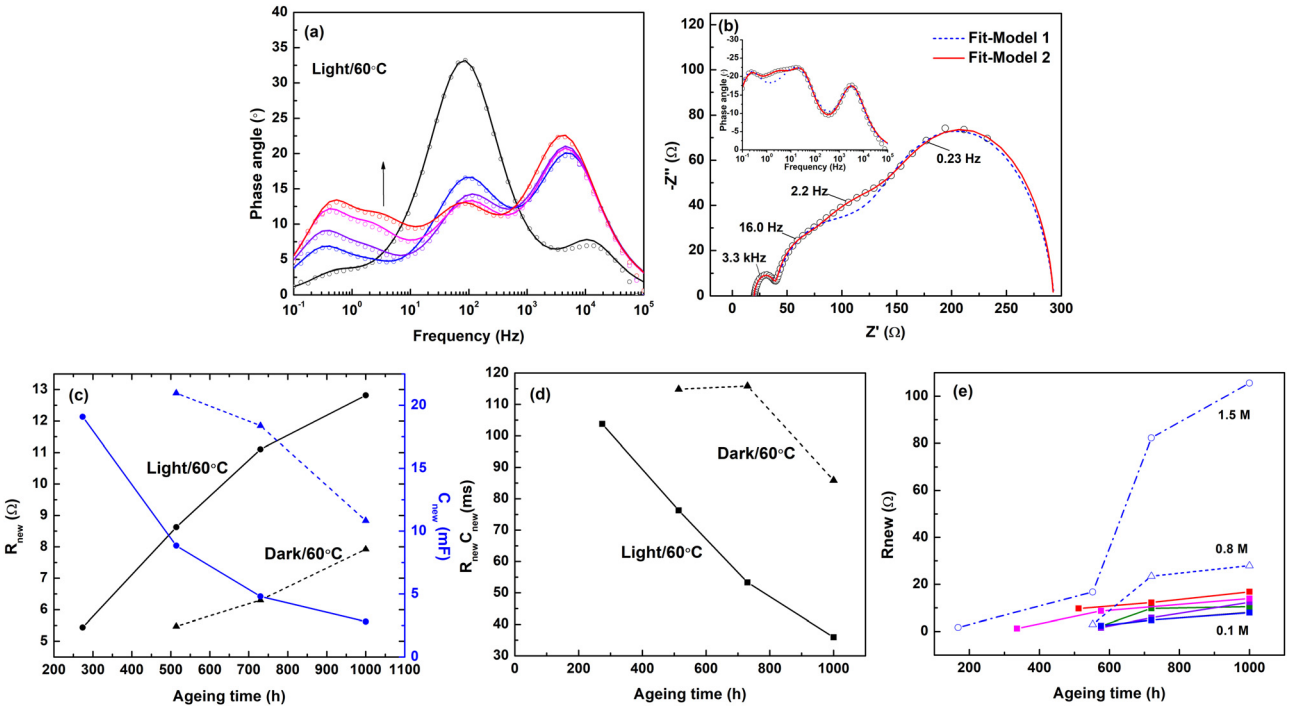

Fig. 2 (a) Bode-phase-angle plots of DSSCs containing 0.1 M EIm^+ aged under light/60 °C for 0 h, black; 274 h, blue; 514 h, purple; 730 h, pink and 1000 h, red. The arrow shows the growth of the new 4th peak. (b) Nyquist plots (inset: Bode phase-angle plots) for DSSCs containing 1.5 M EIm^+ after ageing for 720 h and least-square fitted curves based on different equivalent-circuit models. (c) The evolution of R_{new} (black) and C_{new} (blue) and (d) the evolution of R_{new} C_{new} with ageing time under different ageing conditions: light/60 °C, circle/solid line and dark/60 °C, triangle/dashed line. (e) The evolution of R_{new} with the ageing time for DSSCs containing no (A-free, black) and different cation co-additives of 0.1 M concentration: A-EIm^+, blue solid lines; A-BIm^+, green; A-TBA, purple; A-TEA, pink; and A-Li, red, and EIm^+ of higher concentrations: 0.8 M, blue, triangle, dash line; 1.5 M, blue, circle, dashed dot line. The values were extracted from the corresponding EIS models.

generally observed for all investigated cation co-additive alternatives and shows a clear difference with their types and concentrations.

The new 4th peak indicates the emergence of a new rate-limiting electrochemical process with a time constant that could be distinguished from the other processes. However, the commonly used equivalent-circuit model (model 1 in Scheme 1) cannot accommodate this feature, see Fig. 2b. Therefore, a new RC-circuit element representing a new time constant was added in series to Model 1, and the modified model is denoted as model 2 (Scheme 1). The new resistance and capacitance introduced are denoted as R_{new} and C_{new}, respectively. Based on model 2, the EIS results of aged cells (taking cells containing 1.5 M EIm^+ aged for 720 h as an example) were appropriately modelled and the corresponding results are given in Table S2 (ESI†). Going back to the EIS results of aged cells differing under

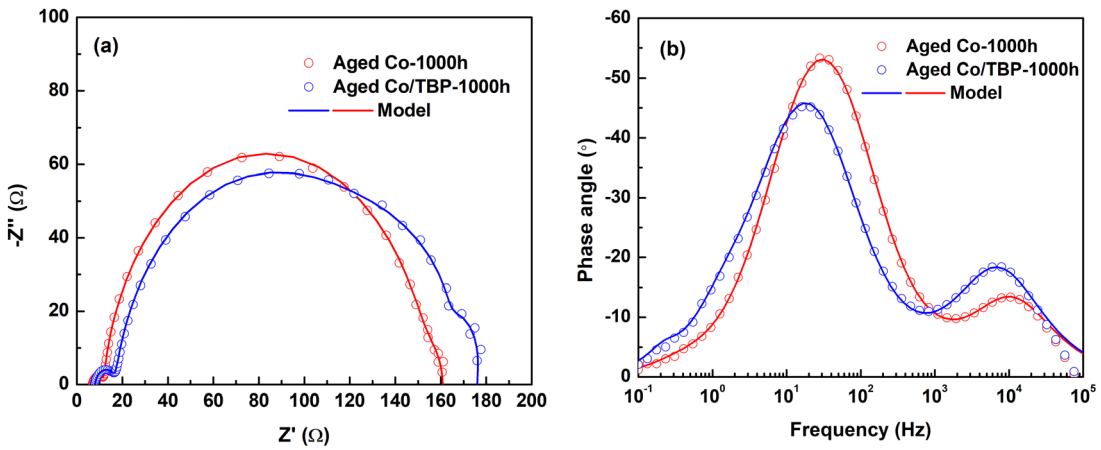

Fig. 3 (a) Nyquist and (b) Bode plots of DSSCs containing different electrolyte components pre-aged for 1000 h before completing the electrolytes and DSSC devices.

the ageing conditions, we can note that R_{new} increases significantly with the ageing time after the first 200–300 hours, and even faster for cells aged under light illumination than for cells kept in the dark (Fig. 2c). Table S3 (ESI†) lists the constant-phase element (CPE) parameters extracted from EIS for both the electron recombination and the new process. The pseudocapacitance Q obtained is generally one or two orders of magnitude higher for the new process (Q_{new}) with respect to that for the typical recombination process (Q_{μ}). The constant phase n is ~ 1 and decreases slightly for the new process as the ageing proceeds. This indicates that the new process can be described by a CPE close to an ideal capacitor. The relaxation process is characterized by a time scale slower than the normal electron recombination and most likely involve charge transfer at a homogeneous electrode surface with a low degree of roughness. According to $C = R^{1/n-1}Q^{1/n}$, the new EIS feature exhibits a high capacitance of several tens of mF and a time constant ($R_{new}C_{new}$) of up to 10^2 ms in the early stage of ageing under light (Fig. 2d). Comparing to the process at the counter electrode characterized by a capacitance at a μF scale and CT at a μs scale, the new EIS feature more likely originates from the TiO_2 surface and is kinetically slower than the previously known electron recombination process. When the ageing proceeds, both C_{new} and the new time constant decreases with time and the decrease is faster for cells aged under light. This means that the transfer of the charge is kinetically accelerated, while the capacity of the charge at the TiO_2 electrode degrades, which leads to an increase in R_{new}.

As shown in Fig. 2e, the increase in R_{new}, which varies with the type of the cobalt co-additives, is larger for strongly coordinating salts with cations of smaller ionic radii (Li^+ and TEA^+) and even more dramatic when increasing the concentration of cation co-additives. The growth of R_{dif} also shows a similar dependency in Fig. S11 (ESI†). It is reasonable to assume that the ion diffusion of cobalt redox complexes, either in the bulk electrolyte or at the electrolyte/TiO_2 interface, must be affected by the addition of cation co-additives and retarded when the amount is high. Also, the effect grows with ageing. In coherence, the increase in R_{new} could possibly result from the diffusion limitation of active species to the working electrode.

Changes within the electrolyte

In light of our previous work, we have recognized that the $Co(bpy)_3^{3+}$-based electrolyte changes upon light ageing and the change only occurs in the presence of the Lewis base additives, such as *tert*-butyl pyridine (TBP).[19,20] By extending the ageing on the electrolyte outside of the device to long times, we can observe a significant linear decrease in the concentration of the original $Co(bpy)_3^{3+}$ based on the ^{1}H-NMR spectroscopic results (Fig. S6 and S7, ESI†). The change was observed to be much less for electrolytes aged in the dark (Fig. S12, ESI†) and none for the solutions containing the dissolved $Co(bpy)_3^{3+}$ salt alone (Fig. S13, ESI†). In parallel, a new paramagnetic cobalt complex, Co′, which give rise to a new peak at 14.5 ppm and must be produced from $Co(bpy)_3^{3+}$, increases with the ageing time. Correspondingly, besides the decrease in the response signal of $Co(bpy)_3^{3+}$, the DPV results also show two new peaks at more positive voltages, indicating that new species are formed during ageing and that are more difficult to oxidize.

Along with these changes, the electrolyte aged *ex-situ* for 1000 h was re-assembled into the DSSC along with fresh electrodes and other non-aged electrolyte components. As shown in Table 2, compared to the electrolyte with $Co(bpy)_3^{3+}$ aged separately, which is actually equivalent to the fresh electrolyte, the one aged together with TBP exhibits a lower V_{oc} and FF. This may be caused by a slightly lower R_{rec} and a higher R_{ct}. Therefore, we can attribute the increase in R_{ct} with the ageing time, which was observed for all investigated systems, to the change within the cell electrolyte and likely to the loss of redox-active Co(III). However, at low frequencies, R_{dif} seems essentially unchanged. This indicates that the gradual deterioration of the ion diffusion for aged cobalt-based cells actually stems from a change at the electrode interface rather than in the bulk electrolyte. The change could occur in the morphology or molecular arrangement at the electrode interface during cell ageing, which influences the ion diffusion at the electrode/electrolyte interface. In contrast, the new EIS feature is still observed for aged Co(III)/TBP electrolytes even assembled with fresh electrodes and the value of R_{new} (28 Ω) is comparable to those of cells aged as a whole device (Fig. 3). This surely suggests that the new EIS feature originates from the composition of an aged electrolyte and that it is the difference in the electrolyte composition that affects the kinetics at the TiO_2/electrolyte interface. Light irradiation causes a more profound change in the aged electrolyte, which well explains the dependence of the new EIS feature on light as mentioned above. The quite high capacitance C_{new} (3.65 mF) of the new EIS feature indicates a high charge-density accumulated at the TiO_2/electrolyte interface and this may suggest that the interaction with a new charged species in the electrolyte is active at the interface. It is thus plausible to suggest that new Co complexes formed during the ageing may be involved, and possibly in the form of oligomers contributing to the high C_{new} characterizing the new process.[21] X-ray absorption spectroscopy

Table 2 The photovoltaic performance and EIS modelling data for DSSCs with different electrolyte components pre-aged for 1000 h before formulating the electrolytes

Aged components[a]	J_{sc}/mA cm^{-2}	V_{oc}/V	FF	η/%	R_{ct}/Ω	C_{ce}/μF	R_{rec}/Ω	C_{μ}/mF	R_{dif}	R_{new}	C_{new}/mF
Co(III)/TBP	10.2	0.93	0.60	5.60	8.8	3.85	123.5	0.23	7.2	28.6	3.65
Co(III)	9.9	0.95	0.63	5.92	4.7	4.13	142.5	0.15	6.6	-	-

[a] Aged in acetonitrile solution under full one sun irradiation (390 nm cut-off filter)/60 °C for 1000 h. Electrolytes were formulated according to the same procedure: 0.22 M/0.05 M $Co(bpy)_3^{2+/3+}$ and 0.2 M TBP in acetonitrile.

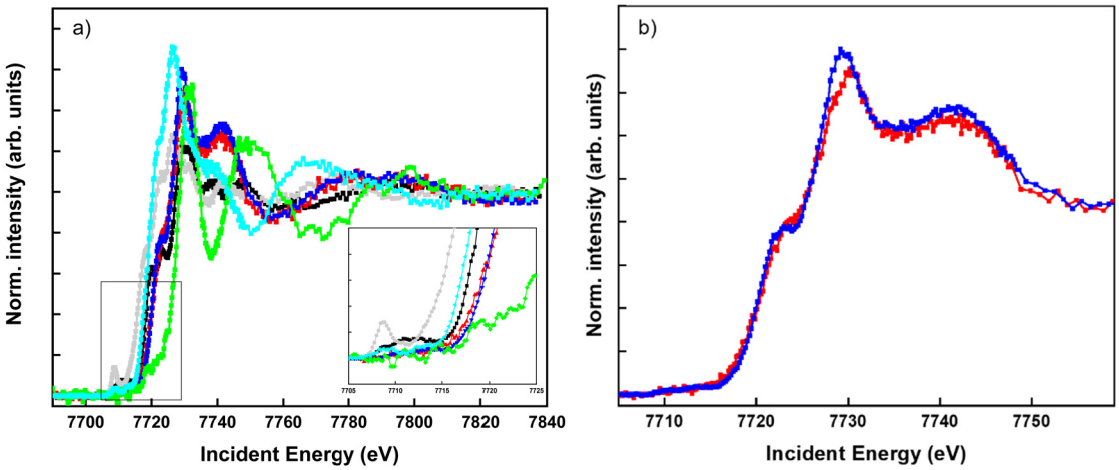

Fig. 4 (a) Co K-edge HERFD-XAS spectra of reference Co compounds along with $Co(bpy)_3^{2+/3+}$ and aged sample. (b) A comparison between fresh $Co(bpy)_3^{3+}$/TBP and aged $Co(bpy)_3^{3+}$/TBP samples, showing a small difference in the chemical state and reordering of ligands. The used samples were CoO, gray line; $LiCoO_2$, black line; low spin $Co(bpy)_3^{2+}$, green line; high spin $Co(bpy)_3^{2+}$, cyan; freshly prepared $Co(bpy)_3^{3+}$/TBP, blue; aged $Co(bpy)_3^{3+}$/TBP, red line.

gives some insights into the Co species formed upon electrolyte ageing.

Transition metal K-edge absorption spectra reveal a strong dependence on the charge distribution and symmetry of the probed site.[22,23] Fig. 4 shows the HERFD-XAS taken at the Co K-edge for a series of $Co^{2+/3+}$ compounds recorded using the K_α emission line compared to reference oxides, as well as low-spin (LS) and high-spin (HS) cobalt reference systems. Two regions of the spectrum can be identified: (i) the K pre-edge from 7705 to 7720 eV and (ii) the K main edge from 7720 to 7840 eV are shown in Fig. 4. The spectral shape and the intensity of the K pre-edge are sensitive to the local site symmetry, while the K main-edge energy position is indicative of the average oxidation state of all absorbing sites.[22,23] The chemical state and changes to the oxidation state of the Co compounds can be determined by observing shifts of the edge energy inflection (E_0), defined as the derivate of the absorption maximum. We found that the main-edge position of $Co(bpy)_3^{2+}$ closely matches with that of the Co^{2+} reference; meanwhile, the $Co(bpy)_3^{3+}$ reference matches the Co^{3+} reference. Upon the addition of TBP to $Co(bpy)_3^{3+}$ and ageing of the sample, the absorption edge remains nearly unchanged (7726.6 eV) for both systems, indicating that the overall oxidation state is preserved (see the inset in Fig. 4).

The effect of ageing of $Co(bpy)_3^{3+}$ shows a change in the spectral profile when compared to $Co(bpy)_3^{3+}$, as shown in Fig. 4(b). The absorption maximum close to 7730 eV shows a small shift for the aged sample compared to the fresh sample, suggesting a partial reduction in the aged sample. The increasing edge is followed by two peaks, the first of which can be ascribed to the dipole allowed transition from Co 1s → 4p levels, while the second one is dominated by single-scattering events involving the absorber (Co) and its N neighbors, likely due to a reordering of the ligand charges as a function of aging the electrolyte. Taken together, this is indicative of a reduction of Co(III) to Co(II) upon ageing associated with also a ligand composition and/or symmetry different from the straightforward product of reduction, $Co(bpy)_3^{2+}$. This may explain the differences observed in the DSSC device performance and the new CT electrode process. More advanced X-ray spectroscopic studies are ongoing in order to attempt to extract more detailed information on the reduced Co species formed upon electrolyte ageing.

Conclusions

In conclusion, EIS is a useful electrochemical tool for studying the ageing effects in DSSCs and has been employed to investigate the degradation and active mechanisms in cobalt-based devices. The performance stability of this type of DSSCs and the related kinetics have been shown to heavily rely on the electrolyte composition. The loss of electrochemically active Co(III), which has been demonstrated to be promoted by light irradiation in the presence of TBP, constitutes the main reason for the DSSC degradation. We have also identified a new EIS feature in long-term aged devices, which is suggested to arise from a new charge-transfer process at the TiO_2/electrolyte interface characterized by relatively slow kinetics and high capacitance. The new process and predominant species involved can be linked to ageing effects in the electrolyte itself, although the effects observed clearly emerge from the electrolyte/TiO_2 interface. XAS indicates a partial reduction of Co(III) in the electrolyte upon ageing, associated also with a different ligand bonding scheme. These fundamental insights highlight the importance of investigating the photochemistry of the electrolyte and the urgency of developing novel characterization techniques allowing a detailed speciation in fresh and aged electrolytes. The results in this study will work as a guide for future efforts on electrolyte optimization for efficient and durable DSSCs.

Author contributions

The manuscript was written by contributions of all the authors. All the authors gave approval to the final version of the manuscript.

Conflicts of interest

The authors declare no competing financial interests.

Acknowledgements

We gratefully acknowledge the Swedish Research Council (2020—681 and 2020-06701), the Swedish Energy Agency and the China Scholarship Council (CSC) for financial support. Qinda Guo and Magnus Hårdensson Berntsen are gratefully acknowledged for valuable scientific discussions.

Notes and references

1 S. Mathew, A. Yella, P. Gao, R. Humphry-Baker, B. F. E. Curchod, N. Ashari-Astani, I. Tavernelli, U. Rothlisberger, K. S. M. Nazeeruddi and M. Grätzel, *Nat. Chem.*, 2014, **6**, 242–247.
2 H. G. Agrell, J. Lindgren and A. Hagfeldt, *Sol. Energy*, 2003, **75**, 169–180.
3 G. Xue, Y. Guo, T. Yu, J. Guan, X. Yu, J. Zhang, J. Liu and Z. Zou, *Int. J. Electrochem. Sci.*, 2012, **7**, 1496–1511.
4 G. Syrrokostas, A. Siokou, G. Leftheriotis and P. Yianoulis, *Sol. Energy Mater. Sol. Cells*, 2012, **103**, 119–127.
5 J. Gao, W. Yang, M. Pazoki, G. Boschloo and L. Kloo, *J. Phys. Chem. C*, 2015, **119**, 24704–24713.
6 S. Mastroianni, I. Asghar, K. Miettunen, J. Halme, A. Lanuti, T. M. Brown and P. Lund, *Phys. Chem. Chem. Phys.*, 2014, **16**, 6092–6100.
7 A. G. Kontos, T. Stergiopoulos, V. Likodimos, D. Milliken, H. Desilvesto, G. Tulloch and P. Falaras, *J. Phys. Chem. C*, 2013, **117**, 8636–8646.
8 R. Jiang, A. Anderson, P. R. F. Barnes, L. Xiao, C. Law and B. C. O'Regan, *J. Mater. Chem. A*, 2014, **2**, 4751–4757.
9 F. Fabregat-Santiago, J. Bisquert, E. Palomares, L. Otero, D. Kuang, S. M. Zakeeruddin and M. Grätzel, *J. Phys. Chem. C*, 2007, **111**, 6550–6560.
10 F. Fabregat-Santiago, J. Bisquert, G. Garcia-Belmonte, G. Boschloo and A. Hagfeldt, *Sol. Energy Mater. Sol. Cells*, 2005, **87**, 117–131.
11 J. I. Basham, T. N. Jackson and D. J. Gundlach, *Adv. Energy Mater.*, 2014, **4**, 1400499.
12 E. Hauff, *J. Phys. Chem. C*, 2019, **123**, 11329–11346.
13 E. Bernhardt, G. Henkel and H. Willner, *Z. Anorg. Allg. Chem.*, 2000, **626**, 560–568.
14 T. Küppers, E. Bernhardt, H. Willner, H. W. Rohm and M. Köckerling, *Inorg. Chem.*, 2005, **44**, 1015–1022.
15 M. Bhagavathi Achari, V. Elumalai, N. Vlachopoulos, M. Safdari, J. Gao, J. M. Gardner and L. Kloo, *Phys. Chem. Chem. Phys.*, 2013, **15**, 17419–17425.
16 L. Simonelli, C. Marini, W. Olszewski, M. Avila Perez, N. Ramanan, G. Guilera, V. Cuartero and K. Klementiev, *Cogent Phys.*, 2016, **3**, 1–10.
17 F. Fabregat-Santiago, G. Garcia-Belmonte, I. Mora-Sero and J. Bisquert, *Phys. Chem. Chem. Phys.*, 2011, **13**, 9083–9118.
18 A. Goossens and J. Schoonman, *J. Electroanal. Chem. Interfacial Electrochem.*, 1990, **289**, 11–27.
19 J. Gao, W. Yang, A. M. El-Zohry, G. K. Prajapati, Y. Fang, J. Dai, Y. Hao, V. Leandri, P. H. Svensson, I. Furó, G. Boschloo, T. Lund and L. Kloo, *J. Mater. Chem. A*, 2019, **7**, 19495–19505.
20 J. Gao, G. K. Prajapati, Y. Hao and L. Kloo, *ACS Appl. Energy Mater.*, 2020, **3**, 5705–5711.
21 J. Gao, A. Fischer, P. H. Svensson and L. Kloo, *ChemistrySelect*, 2017, **2**, 1675–1680.
22 F. De Groot, G. Vankó and P. Glatzel, *J. Phys.: Condens. Matter*, 2009, **21**, 104207.
23 D. Phuyal, S. Mukherjee, S. K. Panda, G. J. Man, K. Simonov, L. Simonelli, S. M. Butorin, H. Rensmo and O. Karis, *J. Phys. Chem. C*, 2021, **125**, 11249–11256.